Cholesterol depletion induces large scale domain segregation in living cell membranes

Mingming Hao*†, Sushmita Mukherjee*, and Frederick R. Maxfield*‡

*Department of Biochemistry, Weill Medical College of Cornell University, New York, NY 10021; and †Department of Chemistry and Chemical Biology, Cornell University, Ithaca, NY 14853

Edited by Marilyn Gist Farquhar, University of California, San Diego, La Jolla, CA, and approved September 6, 2001 (received for review July 19, 2001)

Local inhomogeneities in lipid composition play a crucial role in regulation of signal transduction and membrane traffic. Nevertheless, most evidence for microdomains in cells remains indirect, and the nature of membrane inhomogeneities has been difficult to characterize. We used lipid analogs and lipid-anchored proteins with varying fluidity preferences to examine the effect of modulating cellular cholesterol on domain formation. We show that lowering cholesterol levels induces formation of visible micrometer-scale domains in the plasma membrane of several mammalian cell types with complementary distributions of fluorescent lipid analogs with preferences for fluid or ordered domains. A uniform distribution is restored by cholesterol repletion. Unexpectedly, cholesterol depletion does not visibly alter the distribution of a crosslinked or uncrosslinked glycosylphosphatidylinositol-anchored protein (the folate receptor). We also examined the effect of varying cholesterol content on the cold Triton X-100 solubility of several membrane constituents. Although a cholesterol analog, dehydroergosterol, and a glycosylphosphatidylinositol-anchored protein are largely retained after extraction, a lipid analog with saturated 16-carbon acyl chains is largely removed when the cellular cholesterol level is lowered. This result indicates that after cholesterol depletion molecules in the more ordered domains can be extracted differentially by cold nonionic detergents.

There is strong evidence that biological membranes contain lateral inhomogeneities termed membrane domains (1, 2). However, the data regarding the nature of these domains are mainly indirect. The size, composition, dynamics, and organization of lipid domains in membranes of mammalian cells are largely unknown. Evidence for domains comes in part from examination of membrane constituents that are resistant to solubilization by nonionic detergents at low temperature (3–5). The detergent-resistant membranes (DRMs) are enriched in cholesterol and sphingolipids, which has led to a model for the organization of the plasma membrane in which cholesterol and sphingolipid-rich microdomains (''rafts'') coexist with more fluid domains enriched in phospholipids with unsaturated hydrocarbon chains (2). Despite extensive work on phase separations and the coexistence of multiple phases in model membrane systems (6–8), a relatively simple model of biomembranes containing raft and nonraft domains is widely used to explain many cellular phenomena including aspects of signal transduction processes and membrane trafficking.

The plasma membranes of mammalian cells contain cholesterol (30–50 mol %) and a mixture of lipids with preference for fluid domains (e.g., phosphatidylcholines with unsaturated tails) and lipids with preference for ordered domains (e.g., most sphingolipids; ref. 6). Comparison with studies of model membranes containing cholesterol and two other lipid components has indicated that the lipid properties in DRMs are similar to liquid-ordered (l_o) domains (1, 7–10), which are characterized by tightly packed hydrocarbon tails but with a high degree of lateral mobility. Indeed, DRMs isolated from cells exhibit the properties of l_o domains (11). Cholesterol is thought to contribute to the tight packing of lipids in l_o domains by filling interstitial spaces between lipid molecules (12), and the formation of l_o domains is seen only within certain ranges of cholesterol concentration (1). Effects of cholesterol depletion in cells have been used as evidence for a role for l_o domain-like rafts in various cellular phenomena including signal transduction and membrane traffic (2, 5). For example, a reduction of cholesterol levels blocks both recruitment of a membrane-associated tyrosine kinase, Lyn, to DRMs and activation of signaling (13). This result would be consistent with disruption of rafts as a consequence of cholesterol reduction. However, the effects of cholesterol depletion on the organization of lipids in membranes of living cells have not been investigated fully.

Domain separations have been seen by confocal microscopy of fluorescent lipid analogs incorporated into large unilamellar liposomes (14). Similar experiments in unperturbed mammalian cells have not yielded direct observation of separate domains, leading to the conclusion that domains must be small compared with optical microscopy resolution limits (<250 nm; ref. 15). Large scale perturbations can create observable domains in living cells. A region of ordered lipids was observed when large clusters of IgE receptors were formed by crosslinking (16), and lateral inhomogeneities in lipid distribution were seen as phagosomes were forming (17).

It is possible that the unperturbed membrane has a lipid composition close to the phase-separation boundary for two or more phases. Small changes in physicochemical variables such as cholesterol content, change in lipid head group chemistry, or protein interactions might induce growth or coalescence of certain types of lipid domains. Such a change in turn could initiate membrane-associated physiological phenomena such as signal transduction. In this study we examined the effects of lowering membrane cholesterol on lipid domains in several types of living mammalian cells. We used fluorescent lipid analogs with known partitioning preferences between rigid and fluid membrane domains as tracers to observe the formation and evolution of domains in living cells.

Materials and Methods

Materials. Fluorescent lipid analogs and an Alexa-488 labeling kit were purchased from Molecular Probes. The mouse monoclonal antibody to the human folate receptor, MOv19, was a gift from Centocor. A Cy3 labeling kit was obtained from Amersham Pharmacia. Other chemicals were from Sigma. SIGMAPLOT scientific graphing software was from Jandel (San Rafael, CA).

This paper was submitted directly (Track II) to the PNAS office.

Abbreviations: DRM, detergent-resistant membrane; l_o, liquid ordered; CHO, Chinese hamster ovary; DiI, dialkylindocarbocyanine; C_6-NBD-SM, *N*-{[6-(7-nitrobenz-2-oxa-1,3-diazol-4-yl)amino]hexanoyl}sphingosyl phosphocholine; MβCD, methyl-β-cyclodextrin; DHE, dehydroergosterol; GPI, glycosylphosphatidylinositol; TX-100, Triton X-100.

‡To whom reprint requests should be addressed at: Department of Biochemistry, Weill Medical College of Cornell University, 1300 York Avenue, New York, NY 10021. E-mail: frmaxfie@med.cornell.edu.

The publication costs of this article were defrayed in part by page charge payment. This article must therefore be hereby marked "*advertisement*" in accordance with 18 U.S.C. §1734 solely to indicate this fact.

 www.pnas.org/cgi/doi/10.1073/pnas.231377398

Cells and Cell Culture. TRVb-1 is a modified Chinese hamster ovary (CHO) cell line that lacks endogenous transferrin receptor and expresses the human transferrin receptor (18). FRαTb-1 cells are folate receptor-expressing CHO cells derived from TRVb-1 as described previously (19). All tissue culture media were bicarbonate-buffered and contain FBS, 100 units/ml penicillin, and 100 μg/ml streptomycin. TRVb-1 cells were grown in Ham's F-12 medium supplemented with 2 g/liter glucose, 5% FBS, and 200 μg/ml geneticin (GIBCO) as a selection for the transfected receptors. FRαTb-1 cells were maintained in folate-free Ham's F-12 medium (Specialty Media, Lavellette, NJ) with 5% FBS, 100 μg/ml geneticin, and 200 units/ml hygromycin (Calbiochem). Cells were grown at 37°C in a 5% CO_2 humidified incubator. Except for those treated with metabolic depletion medium, cells were plated 24 h before the experiments in 35-mm plastic tissue culture dishes with a 7-mm hole in the bottom covered by poly-D-lysine-coated coverslips (20).

Labeling Cells with Lipid Analogs. Lipid analogs were transferred as monomers from fatty acid-free BSA carriers (21). Cells were copulsed with 10 μM dialkylindocarbocyanine (DiI)C_{16} or 10 μM $DiIC_{18}$ and 30 μM *N*-{[6-(7-nitrobenz-2-oxa-1,3-diazol-4-yl)amino]hexanoyl}sphingosyl phosphocholine (C_6-NBD-SM) at 37°C for 20 sec, quickly washed with medium 1 (150 mM NaCl, 5 mM KCl, 1 mM $CaCl_2$, 1 mM $MgCl_2$, 20 mM Hepes, and 2 g/liter glucose, pH 7.4), and imaged on a temperature-controlled microscope stage maintained at 33–34°C. The concentrations were chosen to give similar initial intensity. We used the minimum concentration in each case that would give us a useful florescence signal. FRαTb-1 cells were labeled as described previously (19).

Methyl-β-cyclodextrin (MβCD)/dehydroergosterol (DHE) complexes were prepared similarly to a previously described procedure (22), substituting cholesterol with DHE. In brief, DHE in ethanol was dried under argon and subsequently dissolved in 30 mM MβCD in medium 1, making the initial ratio of MβCD to DHE 8:1 (mol/mol). The resulting suspension was vortexed and sonicated until it clarified. It was then incubated in a rocking water bath overnight at 37°C and centrifuged at 21,000 $\times$ *g* for 20 min before labeling cells. The final concentration of DHE used for microscopy was $\approx$1 mM.

Cholesterol Depletion and Repletion. For metabolic depletion, cells were grown for 3 days in metabolic depletion medium (Ham's F-12 medium similar to the growth medium but with 5% lipoprotein-deficient serum in place of FBS, supplemented with 200 μM mevalonate and 10 μM mevastatin) to block cholesterol synthesis and deplete cholesterol stores (23). For depletion by MβCD, cells were incubated with 10 mM MβCD at 37°C for 1 h before labeling. Experiments involving cholesterol repletion were done as follows: cholesterol-depleted cells first were labeled with $DiIC_{16}$ and imaged as described above. Then 10 mM cholesterol-loaded MβCD was added without moving the field. Time-elapsed movies were taken afterward in the presence of cholesterol-loaded MβCD.

Confocal and Epifluorescence Microscopy. Confocal microscopy was performed by using an Axiovert 100-M inverted microscope equipped with an LSM 510 laser scanning unit and an $\times$63 1.4-NA plan Apochromat objective (Zeiss). Cells labeled with red fluorophores ($DiIC_{12}$, $DiIC_{16}$, $DiIC_{18}$, or Cy3-MOv19) were excited with a 1.0-mW helium/neon laser emitting at 543 nm, and a 560-nm long pass filter was used for collecting emissions. Green fluorophores (C_6-NBD-SM or Alexa 488-MOv19) were excited with a 25-mW argon laser emitting at 488 nm, and a 505–530-band pass filter was used for emissions. The two channels were scanned alternately in a line-by-line fashion, having only one laser line and one detector channel on at each time. The fraction of crossover was measured to be less than 5% by using single-labeled samples of each probe (21). The image background was corrected as described previously (24).

Cells labeled with DHE were imaged by using a Leica DMIRB microscope equipped with a Princeton Instruments (Trenton, NJ) cooled charge-coupled device camera driven by IMAGE-1/METAMORPH imaging system software (Universal Imaging, Media, PA). A 335-nm (20-nm bandpass) excitation filter, 365-nm long pass dichromatic filter, and 405-nm (40-nm bandpass) emission filter were used (25) for imaging DHE.

Results

In living cells, a large fraction of $DiIC_{16}$ has been shown to partition into relatively ordered regions of membrane with properties similar to DRMs (16, 17). C_6-NBD-SM is found primarily in the fluid domains because of its short tail with a polar fluorophore at the end. Fig. 1 *A–C* shows cells grown in normal medium in which the plasma membrane is double-labeled with $DiIC_{16}$ (red) and C_6-NBD-SM (green). The cells exhibit relatively uniform labeling with both probes. Similar results have been reported with other markers (26, 27). There are numerous structures that are relatively brightly labeled with both probes, presumably because of surface deformations such as invaginations or filopodia. We do notice, however, that there also are small regions relatively enriched in C_6-NBD-SM that are not enriched in $DiIC_{16}$ (see arrowheads in Fig. 1 *A* and *B*). These small domains are visible above the noise background, and they are observed consistently. This result is illustrated quantitatively in supporting Fig. 5*A* (which is published as supporting information on the PNAS web site, www.pnas.org), in which it is seen that every local increase in $DiIC_{16}$ fluorescence is accompanied by a corresponding increase in C_6-NBD-SM, but some bright patches of C_6-NBD-SM do not have increased DiI fluorescence. These small domains enriched in C_6-NBD-SM might be relatively fluid microdomains within a more ordered background. The small C_6-NBD-SM patches are on the plasma membrane, and they are extracted rapidly by 5% fatty acid-free BSA as the back-exchange medium (24).

When cellular cholesterol levels are reduced metabolically by growing cells in lipid-depleted serum for 3 days, $DiIC_{16}$ and C_6-NBD-SM segregate into domains with complementary patterns (Fig. 1 *D–F*). Identical results are obtained by using $DiIC_{18}$ and C_6-NBD-SM and in two other cell types: normal rat kidney (NRK) and HEp2 human carcinoma cells (data not shown). As a test of cell viability, we measured the efflux kinetics of C_6-NBD-SM, and we find that it is unaffected as described previously (23). A very similar pattern of domain segregation is seen when cholesterol is reduced by a 1-h treatment with a cholesterol-sequestering agent, MβCD (Fig. 1 *G–I*). Furthermore, when energy poisons (NaN_3 and 2-deoxyglucose) are added during cholesterol depletion, lipid rearrangement similar to that shown in Fig. 1 *G–I* is observed again (data not shown). Uptake of transferrin is blocked completely by the energy depletion. This result is consistent with the segregation of domains seen using large unilamellar liposomes (14). We consistently observe enrichment of $DiIC_{16}$ surrounding the C_6-NBD-SM domains, indicating that the boundary regions have properties different from the bulk of the membrane, which remains labeled uniformly with $DiIC_{16}$ (arrows in Fig. 1*D*; ref. 28). Quantitative data on this image are shown in Figs. 5*B* and 6*B* (which are published as supporting information on the PNAS web site).

To be sure that the domain segregation is related to the fluidity preferences of the hydrocarbon tails, we used $DiIC_{12}$, which partitions preferentially into fluid domains because of its short hydrocarbon tails. When $DiIC_{12}$ and C_6-NBD-SM are used to label cholesterol-depleted cells, these two fluid domain-preferring lipids cosegregate into identical domains

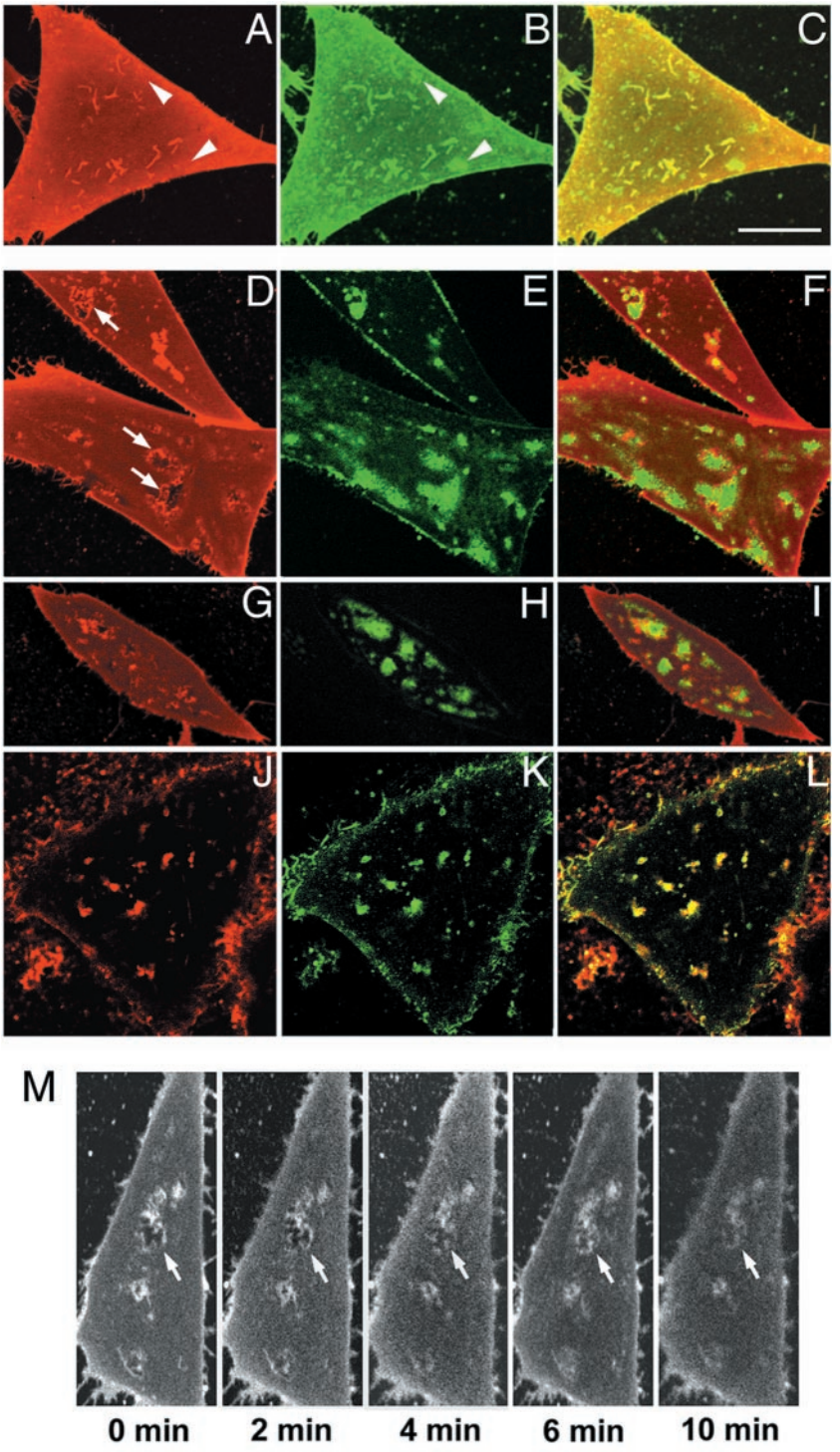

Fig. 1. Effect of cholesterol modulation on the distribution of lipid analogs in the plasma membranes of living CHO cells. The images presented are single confocal sections near the bottom adherent surfaces of living TRVb-1 cells. The lipid analogs used are: *A*, *D*, *G*, and *M*, $DiIC_{16}$ (ordered domain-preferring); *J*, $DiIC_{12}$ (fluid domain-preferring); *B*, *E*, *H*, and *K*, C_6-NBD-SM (fluid domain-preferring); *C*, *F*, *I*, and *L*, red-green overlay. (*A–C*) Cells grown under normal tissue culture conditions and double-labeled with $DiIC_{16}$ and C_6-NBD-SM for 20 sec at 37°C. (*D–L*) Cells in which total cellular cholesterol levels have been depleted to 40% of control levels (estimated by cholesterol oxidase assay using total cell lipid extract) either by growing the cells for 3 days in metabolic depletion medium (*D–F* and *J–L*) or by treating them with the cholesterol-sequestering agent MβCD (*G–I*) before labeling. *M* demonstrates that the distribution pattern shown in *D–I* is a direct result of cholesterol depletion. Cholesterol-loaded MβCD (10 mM) was added to cholesterol-depleted cells pre-labeled with $DiIC_{16}$, and the cells were imaged over a period of 10 min (in 2-min intervals). Stacks of confocal planes were taken to avoid misrepresentation caused by a shift in focal planes (data not shown). (Bar, 10 μm.)

(Fig. 1 *J–L*). It is noteworthy that the fluid domains seen after cholesterol depletion cover only ≈20–30% of the cell surface after quantification (image contrast is adjusted so as to not saturate the brightest pixels). It is clear that the observed domain separation is not what would be expected if small ordered rafts were dispersed after cholesterol depletion. Quantitative data on this image are shown in Figs. 5*C* and 6*C* (which are published as supporting information on the PNAS web site).

Correlation scatter plots based on Fig. 1 *A–L* are presented in supporting Fig. 6 *A–C* (which is published as supporting information on the PNAS web site, www.pnas.org). Fig. 6*A* illustrates the general correlation of $DiIC_{16}$ fluorescence with C_6-NBD-SM as well as the presence of a small number of off-diagonal pixels with bright C_6-NBD-SM in control cells. There is a lack of correlation between $DiIC_{16}$ and C_6-NBD-SM when cholesterol is depleted (Fig. 6*B*), but there is good correlation between $DiIC_{12}$ and C_6-NBD-SM when cholesterol is depleted (Fig. 6*C*).

To test the reversibility of effects of cholesterol depletion, we repleted cholesterol by using cholesterol-loaded MβCD. Domains excluding $DiIC_{16}$ in cholesterol-depleted cells (similar to

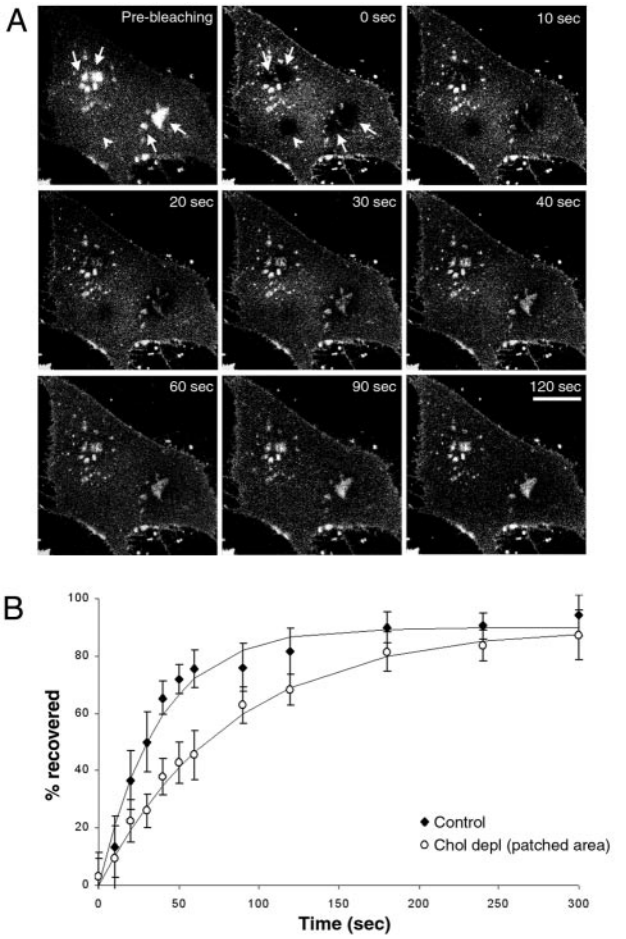

Fig. 2. Fluorescence recovery after photobleaching in cholesterol-depleted cells. (*A*) Cholesterol-depleted cells are labeled with C_6-NBD-SM, and an image is acquired before photobleaching (Pre-bleaching). Several regions of the membrane are photobleached simultaneously for a very brief period by a 25-mW argon laser emitting at 488 nm. Images are taken at different time points after photobleaching to monitor the fluorescence recovery. (Bar, 10 μm.) (*B*) After background correction, a ratio of fluorescence intensities in a photobleached region vs. the entire cell is calculated for each time point. This ratio is divided by the corresponding ratio obtained from the prebleaching image and presented as the percentage recovered in *B*. Each data point, derived from an average of 10 experiments, is fit to the equation $y = y_0 + a(1 - e^{-kt})$ by SIGMAPLOT scientific graphing software, where k is the rate constant.

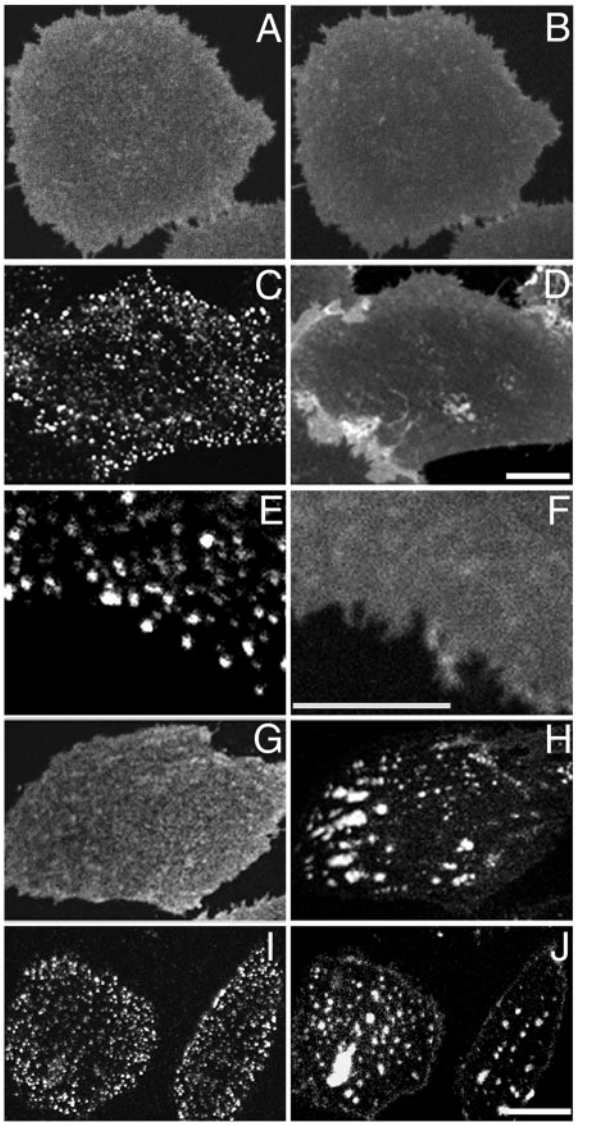

Fig. 3. Role of cholesterol modulation in the domain segregation of GPI-anchored proteins. CHO cells expressing the GPI-linked human folate receptor (FRαTb-1) are grown in either normal growth medium (*A–F*) or cholesterol depletion medium (*G–J*). Cells are double-labeled with Cy3-MOv19, a monoclonal antibody against the human folate receptor (*A*, *C*, *G*, and *I*), with Alexa 488-MOv19 (*E*), $DiIC_{16}$ (*F*), and C_6-NBD-SM (*B*, *D*, *H*, and *J*). Shown in this figure are the cell surface distributions of folate receptors uncrosslinked (*A–B* and *G–H*) and crosslinked by unlabeled polyclonal secondary antibodies (*C–F* and *I–J*). (Bar, 3 μm.)

the ones shown in Fig. 1 *D* and *G*) filled in within minutes after the addition of exogenous cholesterol (Fig. 1*M*).

To determine whether there is diffusional exchange of lipids into and out of the domains enriched in C_6-NBD-SM after cholesterol depletion, we used fluorescence recovery after photobleaching. After bleaching the C_6-NBD-SM in isolated domains in a cholesterol-depleted cell (arrows in Fig. 2*A*), we observed nearly complete recovery of fluorescence with a $t_{1/2}$ of 62 ± 21 sec (Fig. 2 *A* and *B*). This rate is slower than the recovery rate for a region of the same size in control cells ($t_{1/2}$ of 28 ± 14 sec, Fig. 2*B*). When a region relatively depleted of C_6-NBD-SM in cholesterol-depleted cells is photobleached (arrowhead in Fig. 2*A*), fluorescence recovers with a $t_{1/2}$ of 38 ± 18 sec (data not shown). These fluorescence recovery-after-photobleaching results show that although C_6-NBD-SM is present in different concentrations in the fluid and ordered domains after cholesterol depletion, the lipid molecules exchange between these two types of domains relatively rapidly.

Glycosylphosphatidylinositol (GPI)-anchored proteins are a class of lipid-anchored proteins that are associated with DRM fractions, and changes in cholesterol levels affect the distribution and function of GPI-anchored proteins (11, 23, 29, 30). To determine whether the mostly long and saturated tails of GPI-anchored proteins confer properties similar to $DiIC_{16}$, we examined a CHO cell line expressing the human folate receptor (23). When folate receptors are visualized by using a directly labeled monoclonal antibody, they exhibit a relatively uniform distribution similar to C_6-NBD-SM (Fig. 3 *A* and *B*; ref. 31). When the folate receptors are crosslinked by a secondary antibody, they segregate into patches that do not affect the distribution of the fluid-preferring lipid, C_6-NBD-SM (Fig. 3 *C* and *D*; ref. 31). More interestingly, clustering of the crosslinked folate receptor does not alter the uniform distribution of the

CELL BIOLOGY

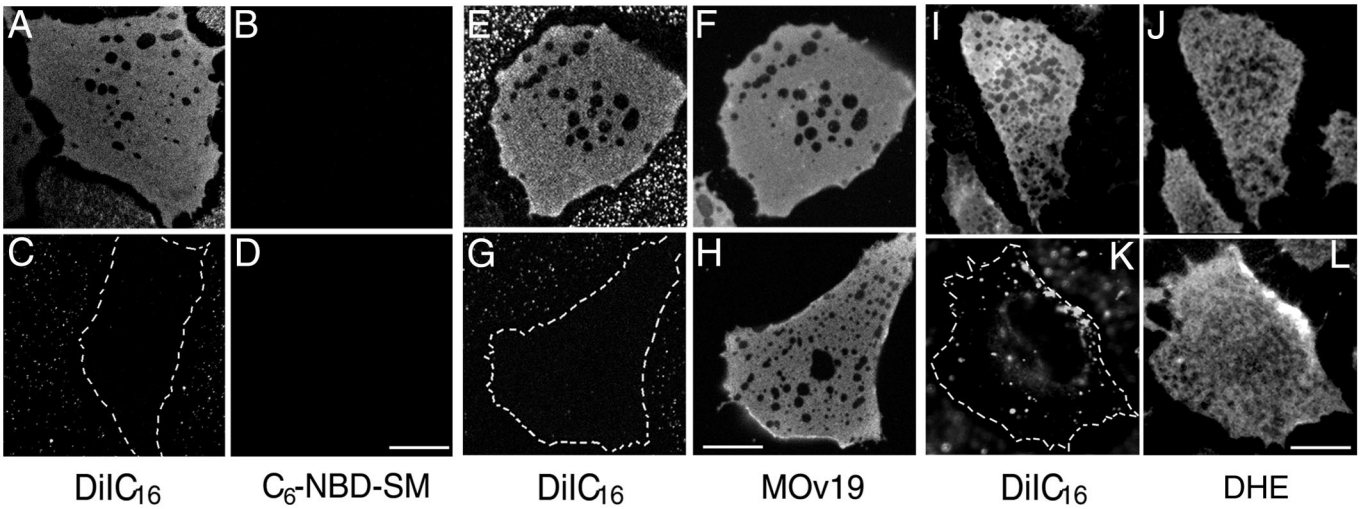

Fig. 4. Cold Triton extractability of $DiIC_{16}$, C_6-NBD-SM, folate receptor, and DHE in normal and cholesterol-modulated cells. TRVb-1 cells first are double-labeled with C_6-NBD-SM and $DiIC_{16}$ at 37°C for 20 sec, washed, and extracted with 1% TX-100 on ice for 30 min (*A–D*). Labeling on ice for 30 min gave the same extraction result (data not shown). For *E–H*, FRαTb-1 cells first are labeled with Alexa 488-MOv19 for 8 min and then labeled with $DiIC_{16}$ for 20 sec at 37°C, washed, and extracted as described above. (*I–L*) Epifluorescence images. TRVb-1 cells first are labeled with DHE for 1 min, washed, and then labeled with $DiIC_{16}$ for 20 sec at 37°C, and extracted as described. *A*, *C*, *E*, *G*, *I*, and *K*, $DiIC_{16}$; *B* and *D*, C_6-NBD-SM; *F* and *H*, Alexa 488-MOv19; *J* and *L*, DHE. In *A–B*, *E–F*, and *I–J* the cells are grown in normal growth medium; in *C–D*, *G–H*, and *K–L* the cells are treated with 10 mM MβCD for 30 min at 37°C before labeling. (Bar, 10 μm.)

order-preferring lipid, $DiIC_{16}$ (Fig. 3 *E* and *F*). A similar result was obtained previously; a GPI-anchored protein (Thy-1) remained diffuse when the folate receptor was clustered by primary and secondary antibodies (31). The clusters of antibody-crosslinked GPI-anchored proteins are ≈100–200 nm in diameter, and they are associated often with caveolae when observed by electron microscopy (31). Transmembrane DRM proteins also were shown to codistribute with each other when they are clustered (32). When large (>1-μm) clusters of IgE receptors were formed on rat basophilic leukemia cells, $DiIC_{16}$ became enriched under the crosslinked IgE receptors at low temperature (16). Taken together these results indicate that the formation of specialized domains by crosslinking one DRM component induces only a weak preference for monomers of a second DRM component to become enriched there. In some cases, factors such as clustering of raft-like domains through protein crosslinking might contribute to the recruitment of a second component to the same DRM.

Unexpectedly, cholesterol depletion does not alter the distribution of either the uncrosslinked or crosslinked folate receptor to an extent similar to the lipid redistribution (Fig. 3 *G–J*; compare Fig. 1 *D–I*). The folate receptor in cholesterol-depleted cells has a slightly granular and less diffuse distribution compared with that in untreated cells (Fig. 3 *A* and *G*). The difference is subtle but consistently observed. In addition, the clustered GPI-anchored proteins in cholesterol-depleted cells overlap both the regions that contain C_6-NBD-SM and the regions that exclude this fluid probe (Fig. 3 *I* and *J*). The two probes show a near random correlation in supporting Fig. 6*D*. This result, along with the aggregation experiment described above, shows that different molecules that associate with DRMs can have different distribution properties when probed by a second type of membrane perturbation (i.e., cholesterol depletion).

We characterized further the similarity and difference of domains defined by differential partitioning of lipid analogs vs. those defined by insolubility in cold Triton X-100 (TX-100). When cells labeled with $DiIC_{16}$ and C_6-NBD-SM are extracted with cold TX-100 *in situ*, we find that most of the surface area remains labeled by $DiIC_{16}$, and in each cell there are several extracted holes up to a few micrometers in diameter (Fig. 4*A*). These results are very similar to the extraction pattern of GPI-anchored proteins by cold TX-100 (Fig. 4*F*; ref. 19). Along with the cholesterol depletion experiments conducted at 37°C (Fig. 1 *D–L*), the cold TX-100 extraction indicates that most of the plasma membrane surface area is detergent-resistant. C_6-NBD-SM (Fig. 4 *B* and *D*) and $DiIC_{12}$ (data not shown) were extracted completely by cold TX-100 under all conditions.

We compared the cold TX-100 insolubility of three DRM components, $DiIC_{16}$, the folate receptor, and DHE, in cells with different cholesterol content. DHE is a naturally fluorescent sterol with distribution properties very similar to cholesterol (25, 33). All three DRM components show a very similar pattern of large holes in cells after cold TX-100 extraction (Fig. 4 *E*, *F*, *I*, and *J*). We find that the properties of the ordered domains are altered by cholesterol depletion. When cholesterol is reduced by MβCD treatment (Fig. 4 *C*, *D*, *G*, *H*, *K*, and *L*) or metabolically (data not shown), most of the $DiIC_{16}$ is extracted by cold TX-100 (Fig. 4 *C*, *G*, and *K*). In contrast, the folate receptor (Fig. 4*H*) and DHE (Fig. 4*L*) remain largely insoluble in cold TX-100 after cholesterol depletion. This result indicates that after cholesterol depletion, molecules in the more ordered domains can be differentially extracted by detergent.

Discussion

Although it is widely accepted that the plasma membrane contains lateral inhomogeneities (i.e., microdomains), the properties of these domains remain uncertain. The size, duration, and number of types of domains are not known. In a simplified version of the raft model, the plasma membrane can be thought of as coexisting l_o (raft) and fluid (nonraft) domains. It often is assumed that rafts are the minor component, and molecules can become concentrated significantly by recruitment to rafts (e.g., in some signal transduction complexes). Because l_o domains require cholesterol, the effects seen after cholesterol depletion are interpreted often as being a consequence of raft disruption. Within this paradigm, resistance to solubilization in cold, nonionic detergents is taken as an indication of inclusion in rafts. In this paper we observed directly the properties of fluorescent lipid analogs with differing preferences for fluid or ordered domains.

We compared the effects of cholesterol depletion and treatment with cold TX-100 with the predictions of a simple raft model.

In unperturbed cells, we see small domains in which fluid-preferring C_6-NBD-SM is enriched compared with $DiIC_{16}$ (Figs. 1 *A–C* and supporting Figs. 5*A* and 6*A*). When cholesterol levels are reduced, we observe domains in mammalian cells that seem to arise by lipid-lipid immiscibility (34). These domains are stable for tens of minutes and are hundreds of nanometers to microns in length. The boundaries between the more ordered and fluid domains in cholesterol-depleted cells seem to have unique partitioning properties (see arrows in Figs. 1*D* and supporting Fig. 5*B*). Although the detailed mechanism of formation of these large domains will require further investigation, one interpretation is that cholesterol may stabilize boundaries between microdomains such that the removal of cholesterol leads to coalescence of microdomains into observable micrometer-scale domains. In any case, the observed effects of cholesterol depletion differ from a prediction of disruption of small rafts.

There seem to be several types of domains in the same cell, one of which is caveolae that contain the crosslinked folate receptors with no detectable exclusion or enrichment of C_6-NBD-SM or $DiIC_{16}$ (Fig. 3 *C–F*). In cholesterol-depleted cells the C_6-NBD-SM and $DiIC_{16}$ separate into distinct domains (Fig. 1 *D–I*), but the GPI-anchored proteins are in both domains even when crosslinked (Fig. 3 *G–J*). These data indicate that useful models of the properties of lipids must take into account multiple types of domains in the plasma membrane. Furthermore, components that share one property (i.e., resistance to cold TX-100) will nevertheless distribute differentially among domains.

Our data support the idea that most of the plasma membrane of mammalian cells is in a more ordered state with properties that have been attributed to rafts including resistance to cold TX-100 and a high content of sterols. Therefore, instead of having a few rafts of ordered lipids in a sea of fluid lipids, it might be more accurate to envision a membrane that is mostly rafts with small regions of fluid lipids intercalated among mostly ordered lipid domains. Because many important cellular events such as signaling require the coalescence and possible reorganization of certain types of domains, cholesterol-dependent domains similar to those reported in this paper can play important roles in the modulation of critical cellular phenomena.

We thank Drs. Timothy McGraw, Sharron Lin, and Lynda Pierini for helpful discussions and critical reading of the manuscript. This work is supported by National Institutes of Health Grant DK 27083.

1. Brown, D. A. & London, E. (2000) *J. Biol. Chem.* **275,** 17221–17224.
2. Simons, K. & Ikonen, E. (1997) *Nature (London)* **387,** 569–572.
3. Brown, D. A. & Rose, J. K. (1992) *Cell* **68,** 533–544.
4. Brown, D. A. & London, E. (1998) *J. Membr. Biol.* **164,** 103–114.
5. Roper, K., Corbeil, D. & Huttner, W. B. (2000) *Nat. Cell Biol.* **2,** 582–592.
6. Gennis, R. B. (1989) in *Biomembranes: Molecular Structure and Function* (Springer, New York), pp. 20–32.
7. Sankaram, M. B. & Thompson, T. E. (1991) *Proc. Natl. Acad. Sci. USA* **88,** 8686–8690.
8. Silvius, J. R., del Giudice, D. & Lafleur, M. (1996) *Biochemistry* **35,** 15198–15208.
9. Ahmed, S. N., Brown, D. A. & London, E. (1997) *Biochemistry* **36,** 10944–10953.
10. Ge, M., Field, K. A., Aneja, R., Holowka, D., Baird, B. & Freed, J. H. (1999) *Biophys. J.* **77,** 925–933.
11. Schroeder, R. J., Ahmed, S. N., Zhu, Y., London, E. & Brown, D. A. (1998) *J. Biol. Chem.* **273,** 1150–1157.
12. Brown, R. E. (1998) *J. Cell Sci.* **111,** 1–9.
13. Field, K. A., Holowka, D. & Baird, B. (1995) *Proc. Natl. Acad. Sci. USA* **92,** 9201–9205.
14. Korlach, J., Schwille, P., Webb, W. W. & Feigenson, G. W. (1999) *Proc. Natl. Acad. Sci. USA* **96,** 8461–8466.
15. Varma, R. & Mayor, S. (1998) *Nature (London)* **394,** 798–801.
16. Thomas, J. L., Holowka, D., Baird, B. & Webb, W. W. (1994) *J. Cell Biol.* **125,** 795–802.
17. Pierini, L., Holowka, D. & Baird, B. (1996) *J. Cell Biol.* **134,** 1427–1439.
18. McGraw, T. E., Greenfield, L. & Maxfield, F. R. (1987) *J. Cell Biol.* **105,** 207–214.
19. Mayor, S. & Maxfield, F. R. (1995) *Mol. Biol Cell* **6,** 929–944.
20. Salzman, N. H. & Maxfield, F. R. (1989) *J. Cell Biol.* **109,** 2097–2104.
21. Mukherjee, S., Soe, T. T. & Maxfield, F. R. (1999) *J. Cell Biol.* **144,** 1271–1284.
22. Sheets, E. D., Holowka, D. & Baird, B. (1999) *J. Cell Biol.* **145,** 877–887.
23. Mayor, S., Sabharanjak, S. & Maxfield, F. R. (1998) *EMBO J.* **17,** 4626–4638.
24. Hao, M. & Maxfield, F. R. (2000) *J. Biol. Chem.* **275,** 15279–15286.
25. Mukherjee, S., Zha, X., Tabas, I. & Maxfield, F. R. (1998) *Biophys. J.* **75,** 1915–1925.
26. Maxfield, F. R. & Mayor, S. (1997) *Adv. Exp. Med. Biol.* **419,** 355–364.
27. Rock, P., Allietta, M., Young, W. W., Jr., Thompson, T. E. & Tillack, T. W. (1990) *Biochemistry* **29,** 8484–8490.
28. Louraab, L. M., Fedorova, A. & Prietoa, M. (2000) *Biochim. Biophys. Acta* **1467,** 101–112.
29. Brown, D. A. & London, E. (1997) *Biochem. Biophys. Res. Commun.* **240,** 1–7.
30. Hoessli, D. C. & Robinson, P. J. (1998) *Trends Cell Biol.* **8,** 87–89.
31. Mayor, S., Rothberg, K. G. & Maxfield, F. R. (1994) *Science* **264,** 1948–1951.
32. Harder, T., Scheiffele, P., Verkade, P. & Simons, K. (1998) *J. Cell Biol.* **141,** 929–942.
33. Schroeder, F., Barenholz, Y., Gratton, E. & Thompson, T. E. (1987) *Biochemistry* **26,** 2441–2448.
34. Rietveld, A. & Simons, K. (1998) *Biochim. Biophys. Acta* **1376,** 467–479.